Soft Matter

Accepted Manuscript

Volume 1 | Number 1 | Jan 2013 | Pages 1–100

Soft Matter

www.rsc.org/softmatter

ROYAL SOCIETY OF CHEMISTRY

ROYAL SOCIETY OF CHEMISTRY

www.rsc.org/softmatter

Filler-Rubber Interface in Styrene Butadiene Nanocomposites with Anisotropic Silica Particles. Morphology and Dynamic Properties.

L. Tadiello,[a] M. D'Arienzo,[a] B. Di Credico,[a] T. Hanel,[b] L. Matejka,[c] M. Mauri,[a] F.Morazzoni,[a] R. Simonutti,[a] M. Spirkova,[c] R. Scotti[a]*

[a] Dip. Scienze dei Materiali, INSTM, University of Milano-Bicocca, Via R. Cozzi, 55, 20125 Milano, Italy; [b] Pirelli Tyre SpA, Viale Sarca 222, 20126 Milano, Italy; [c]Institute of Macromolecular Chemistry, Academy of Science of the Czech Republic, Heyrovskeho Nam. 2, Prague, Czech Republic.

ABSTRACT Silica/Styrene Butadiene Rubber (SBR) nanocomposites were prepared by using shape-controlled spherical and rod-like silica nanoparticles (NPs) with different aspect ratios (AR=1-5), obtained by sol-gel route assisted by a structure directing agent. The nanocomposites were used as models to study the influence of the particle shape on the formation of nanoscale immobilized rubber at the silica-rubber interface and its effect on the dynamic-mechanical behavior. TEM and AFM tapping mode analyses of nanocomposites demonstrated that the silica particles are surrounded by a rubber layer immobilized at the particle surface. Spherical filler showed small contact zones between neighboring particles contacting thin rubber layers, while anisotropic particles (AR >2) formed domains of rods preferentially aligned along the main axis.

A detailed analysis of the polymer chain mobility by different time domain nuclear magnetic resonance (TD-NMR) techniques evidenced a population of rigid like rubber chains surrounding particles, whose amount increases with the particle anisotropy, even in the absence of significant differences in terms of chemical crosslinking. Dynamic measurements demonstrate that rod-like particles induce stronger reinforcement of the rubber, increasing with the AR. This was related to the self-alignment of the anisotropic silica particles in domains able to immobilize rubber.

Introduction

The addition of filler nanoparticles (NPs) is the main strategy to improve the mechanical properties of elastomers.[1-4] The tire industry extensively employs carbon black and silica particles to increase abrasion resistance and wet grip and to reduce the rolling resistance.[5]

In the last decades many experimental and theoretical studies have regarded the complex mechanism by which fillers modify the rubber macro scale mechanical properties.[6-7] Different contributions have been proved to give rise to the rubber reinforcement: the hydrodynamic effect, the polymer network, the interparticle filler-filler and the interface filler-rubber interactions.[8] These determine the formation of the percolative filler network in the rubber matrix, that is essential for providing effective reinforcement.

In particular, the crucial importance of the filler-rubber interaction has been recognized to control the filler dispersion and networking through the polymer matrix[8, 9], depending on the filler size and on the polymer and filler surface chemistry.[10, 11] Nevertheless, the knowledge of the exact mechanism at the microscopic scale by which the filler rubber interaction affects the mechanical reinforcement is still one of the main topics of current investigation[10-12] and the influence of the inorganic/organic interface on the mechanical behavior still remains a challenge.

The prevailing theory considers that the mechanical reinforcement is related to the strength of the particle-rubber interaction at the organic/inorganic interface, and identifies a "bound rubber" phase to describe such interaction.[13, 14] The bound rubber is defined as a polymer film of a few nanometers[12-16] fixed at the particle rubber interface and thus resistant to dissolution in solvent. More in detail, this film was described as a primary layer of tightly bound rubber interacting with the filler through Van der Waals or chemical bonds (*e.g.* via silane coupling agents) and a secondary rubber layer more loosely bound to the primary one.[17, 18]

Within these layers the motion of polymer chains is restricted, the rubber stiffness increasing in comparison with the free rubber far from the particles. The stronger the interaction, the more tied the polymer layer is.[15-19] According to this model, the interaction between filler NPs is provided by the overlap of the rigid rubber layers.[13-16]

Rubber occluded inside the particle aggregates[20-21] has also been considered as a component of the bound rubber other than that due to direct filler rubber interaction. This rubber contributes to the modulus at low strain since it is constrained in the voids of particle aggregates and is released by increasing the rubber deformation.[8, 20, 21]

The existence of rubber chains with reduced mobility close to filler particles has been already revealed in carbon black,[12, 20, 21] layered silicates[22, 23] and silica[15-19] filled elastomers, and it has been studied by different approaches. Low field ^{1}H Nuclear Magnetic Resonance (NMR) spectroscopy has been used to measure the T_2 relaxation time of chains with restricted mobility;[24-26] Atomic Force Microscopy (AFM) images evidenced the topography and thickness of the rigid rubber,[12, 27] and torsional harmonic AFM has been successively applied to locally determine the stiffness.[12, 28] Moreover, many atomistic or coarse-grained simulations [29-32] and non equilibrium thermodynamics models[33] have been proposed to study the microstructure of

polymers filled with nanoparticles and gave a rationale to low mobility of the polymer chains interacting with them.

The amount of rigid rubber strongly depends on the area and the nature of the filler rubber interface, and on the presence of physical constraints [34-38]. However, the influence of the particle morphology and/or of their anisotropy has been rarely systematically considered, particularly in the case of silica[39]. This is probably due to the difficulty of obtaining anisotropic shape controlled NPs. To the best of our knowledge, no research has reported about the influence of the silica NP shape on the kind and amount of rigid rubber, either directly interacting with the surface of the filler particles or physically occluded in particle aggregates. We recently succeeded in the preparation of styrene butadiene rubber (SBR) nanocomposites containing shape controlled anisotropic NPs with different aspect ratios (ARs)[40]. This allowed varying the mechanical properties of the nanocomposites, where the highest reinforcing properties result associated to the highest AR (*i.e.* 2-7) particles. The increase of the reinforcing effect of the rod-like particles by increasing their AR was related to both the self-alignment of anisotropic particles along the major axis direction and to their very large filler/polymer interface, compared to that of spherical particles.

The aim of the present work is to further investigate the influence of the anisotropic silica particles on the dynamic-mechanical behavior of the SBR nanocomposites, mainly considering the formation of the nanoscale rigid rubber at the interface with the filler.

Shape controlled silica NPs with AR ranging from 1 to 5 were used to prepare *ex-situ* blended silica/SBR nanocomposites. In order to highlight the effect of the particle shape, the same graft density of bis (3-triethoxysilylpropyl) disulfide (TESPD) present as coupling agent was used for all the prepared compounds.

The morphology of the nanocomposites and the topography of the rigid rubber were investigated by the integrated approach of Transmission Electron Microscopy (TEM) with AFM, to visualize the stiffest elastomer zone at the interface. Low field ^{1}H NMR measurements were performed using Magic Sandwich Echo (MSE) to investigate the mobility of rubber chains close to the filler particles, distinguishing between the motional regimes of tightly and more loosely interacting and free rubber chains. Finally, Dynamic Mechanical Thermal Analysis (DMTA) assessed the fraction of rubber with reduced mobility[41-42] which affects the stress/strain behavior of cured silica/SBR nanocomposites, and tensile stress-strain tests allowed to study the behavior under high deformation.

2. Experimental

2.1. Materials

Silica synthesis: tetraethoxysilane, TEOS, (99%), (3-mercaptopropyl)trimethoxysilane, MPTMS, (95%), cetyltrimethylammonium bromide, CTAB, (98%), were purchased from Aldrich and were used without further purification. Milli-Q water was used with a resistivity >18.2 MΩ•cm. Compounding: SBR, was SLR 4630 from Styron Europe GmbH (25% styrene; 63% vinyl; 12% butadiene; 37.5 parts of Treated Distillate Aromatic Extract (TDAE) extender oil); TESPD, was purchased from Aldrich; N-(1,3-dimethylbutyl)-N'- phenyl-p-phenylendiamine, 6PPD, used as antidegradant was Santoflex-6PPD from Flexsys; stearic acid was Stearina TP8 from Undesa; sulfur was from Zolfoindustria; zinc oxide was from Zincol Ossidi; N-cyclohexyl-2-benzothiazole sulfenamide, CBS, was Vulkacit CZ/C from Lanxess.

2.2. Sol-gel synthesis of silica NPs

Shape-controlled silica NPs were prepared according to the method reported elsewhere[43] to obtain spherical or rod-like silica NPs having different ARs (1, 2.5, 5 respectively). Hereafter, the different shaped silica particles will be labeled SX, where X refers to the ARs of the silica particles (X = 1 spherical shape; X = 2 and 5, rod-like shape).

As reported in a previous paper[40], S1 are spherical, with ~ 80 nm of diameter, or slightly elongated with cross section of ~ 80 nm and 120 ± 20 nm length; S2 are elongated, with cross section of 80 ± 10 nm and the longest dimension 200 ± 40 nm (AR, ~ 2.5); S5 are rod-like shaped with 70 ± 10 nm cross section and length of 380 ± 80 nm (AR ~ 5). The density of silica in SX samples was measured by a helium pycnometer is 1.74 ± 0.02 g·cm^{-3}. BET specific surface area (SSA) resulted very large (S1, 1107 m^2/g; S2, 1050, m^2/g; S5 1336 m^2/g) due to the high mesoporosity[40].

2.3. Preparation and curing of silica/SBR nanocomposites

Uncured composite materials were prepared by mixing SBR with 12, 25 and 35 phr (part per hundred rubber) of SX and, respectively, 1.0, 2.0 and 2.8 phr of TESPD in a Brabender Plasti-Corder lab station internal mixer (65 mL mixing chamber, 0.6 filling factor), working at temperature of 135 °C. Hereafter, uncured nanocomposites will be labeled SBR-SX-W, where X stands for the SiO$_2$ particle AR and W for silica loading in phr.

Vulcanization chemicals were then added to the obtained composites in two steps. First, 3.5 phr of ZnO, 2.5 phr of 6PPD and 1 phr of stearic acid were fed to the same mixer with SBR-SX-W and mixed at 90 °C, 70 rpm for 6 min. Successively, 1 phr of S and 3 phr of CBS were added, performing a successive mixing step at 90 °C for 4 min in a two-roll mill. Composites were further molded for 2 min to produce sheets of about 2 cm thick, suitable for the vulcanization process. Finally, cured composites containing 12, 25 and 35 phr of SX were obtained by

vulcanization of SBR-SX-W performed in a hydraulic press at 170 °C and under the pressure of 200 bar for 20 min. Cured samples will be called V-SBR-SX-W in the following.

A reference material without any filler was prepared and labeled SBR-REF-0 and V-SBR-REF-0. Curing profiles of uncured composites were measured with a Moving Die Rheometer (RPA 2000, Alpha Technological) under the following conditions: ±1° oscillation angle, 170 °C temperature, 4.3 bar pressure and 30 min running time. This analysis gave the optimum conditions for the curing of composites.

2.4 Characterization of silica/SBR nanocomposites

The degree of functionalization of SX with TESPD was estimated by TGA measurements on SX powder mixed with TESPD at the same temperature of the compounding treatment. The thermal profile was obtained at constant N_2 flow (50 ml min^{-1}) by heating rate 5 °C min^{-1} in the range 30–150°C and at constant air flow (50 ml min^{-1}) by heating rate 10 °C min^{-1} in the range 150–1000 °C. The amount of TESPD grafted to silica was calculated by the difference between the weight loss of SX powders mixed with TESPD in the interval 150-1000 °C and that of pure SX, where the loss derived from the removal of surface OH and alkylthiol groups residual from the synthesis procedure. In all samples the amount of TESPD bound to silica resulted in agreement with the nominal values (see paragraph 2.3).

 The morphological investigation of vulcanized composites was carried out by TEM using the Zeiss EM 900 microscope. Ultrathin sections (about 50 nm thick) of composites were obtained with a Leica EM FCS cryo-ultramicrotome equipped with a diamond knife, by keeping the samples at −130 °C. The thickness of the specimens (~ 40 nm) can cause the longest silica particles to be cut, depending on their orientation. Thus, the presence of some particles anomalously shorter and thinner compared to the size dimensions of SX (see paragraph 2.3) may

be due to the sectioning of the samples.

Investigation of the topography and the heterogeneity relief, on nanocomposites previously freeze-fractured at the temperature of liquid nitrogen, was done by atomic force microscope (Dimension Icon, Bruker), equipped with the SSS-NCL probe, Super Sharp SiliconTM - SPM-Sensor (NanoSensorsTM Switzerland; spring constant 35 N m^{-1}, resonant frequency ≈ 170 kHz). Measurements were performed under ambient conditions using the tapping mode AFM technique. The scans covered the sizes from 1×1 to 50×50 μm^2. Roughness is described in Table S1 of Supporting Information.

Time Domain NMR experiments were carried out on a Bruker Minispec mq20 spectrometer operating at around 0.5 T static magnetic field, with proton resonance of 19.65 MHz, π/2 pulse length between 2.05 and 2.20 μs, phase switching time around 2.1 μs and receiver dead time τ set at 14 μs. Samples were prepared by inserting in 10 mm outer diameter tubes a quantity of rubber chunks sufficient to fill the region of maximum magnet homogeneity (about 8 mm height), where the sample was then carefully centered. Estimation of the rigid fraction was obtained by acquiring MSE refocused Free Induction Decay (FID)[44] and applying a proper back correction for the inherent inefficiency of the sequence[45]. The weight/weight proton content was measured by the intensity I_o of the FID normalized to the mass w using a calibration line in accordance with a previously reported quantitative procedure ("proton counting")[25, 46]. MSE and proton counting experiments were well accumulated with less than 128 scans. Recycle delays of 1-2 s provided full relaxation in all materials. MSE experiments were performed also on pure silica in order to measure the rigid proton fraction in the filler. To this purpose, SX samples were dried in vacuo at 100 °C and a paste was prepared for the measurements by mixing them with D_2O in a Schlenk manifold.

The ratio between this value and the percentage of all rigid protons in V-SBR-SX-W, as obtained by MSE measurements, gives the fraction of rigid protons attributed to SX ($f_{r\,(SiO2)}$). The real fraction of rigid protons due to the rubber in V-SBR-SX-W ($f_r{*}$) was calculated by subtracting $f_{r\,(SiO2)}$ from the total fraction of rigid proton f_r obtained by MSE. After this correction, $f_r{*}$ in V-SBR-SX-W corresponds to the true fraction of rigid rubber.

Blank experiments were also performed on unfilled V-SBR-REF, as prepared and with the addition of the coupling agent TESPD. The difference between the two samples is negligible and demonstrates that TESPD alone in rubber does not affect the rigid proton population.

2.5 Dynamic Mechanical Analysis

DMTA of V-SBR-SX-W was performed by an Ares G2 apparatus (TA Instruments) by applying a shear stress mode. The temperature dependence of the complex shear modulus of rectangular samples (5 x 1 x 0.25 cm^3) was measured by oscillatory shear deformation at a frequency of 1 Hz and at the heating rate of 3 °C min^{-1}.

2.6. Tensile tests

Tensile tests were carried out using an Instron 5800 apparatus at 25 °C and a crosshead speed of 50 mm/min^1. Investigation of the prestrained composites was performed to follow the so called Mullins strain softening effect[47, 48]. A set of extension-retraction cycles was carried out, and the equilibration time between each cycle was 30 minutes.

3. Results and discussion

3.1 TEM and AFM morphological analysis

TEM investigation of V-SBR-SX-35 samples was reproduced and here reported, although shown in a previous paper[40], in order to more easily discuss the effects of the particle anisotropy on the rubber matrix (Figure 1). V-SBR-S1-35 contains spherical or near spherical particles with

uniform particle distribution and continuous network. The network appears less continuous by increasing the AR (i.e. V-SBR-S2-35 and V-SBR-S5-35 composites). In all samples, silica particles are surrounded by rubber layers. Moreover, when AR increases (AR≥2) a preferential alignment of particles occurs along their main axis, which is more evident for the longest rods in V-SBR-S5-35. This leads to the formation of domains of few aligned nanoparticles whose orientation in the rubber matrix is different. The alignment was attributed to the interaction between the larger interface of the anisotropic particles compared to that of the spherical ones[40].

Lower filler loading composites V-SBR-SX-12 were also investigated (not reported). The particles resulted highly dispersed in the rubber matrix, separated by a large distance and without any alignment[40].
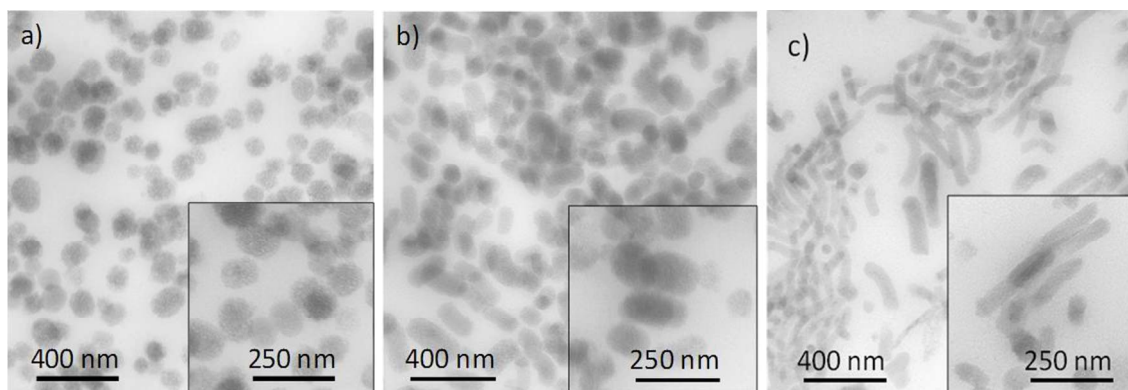
Figure 1. TEM images of cured V-SBR-SX-35 composites: a) V-SBR-S1-35; b) V-SBR-S2-35; c) V-SBR-S5-35

The nanocomposite morphology and the rubber/particle interface were investigated by AFM. The analysis was performed in tapping mode on fresh surfaces after freeze-fracturing the materials. 3D height images were compared with 2D amplitude error images, which show sharper contrast at the edges of the heterogeneous zones of the materials and give better evidences of the interface regions (Figure 2). V-SBR-S1-35 3D image (Figure 2 a) shows

homogeneous dispersion of particles, with small contact zone between the neighboring ones. This distribution is similar to that reported in the literature for spherical silica particles in rubber nanocomposites and described as string-of-pearls[49, 50]. 2D amplitude error image (Figure 2 a') evidences well distinguishable rubber layers around particles, slightly overlapping at the particle contact points.
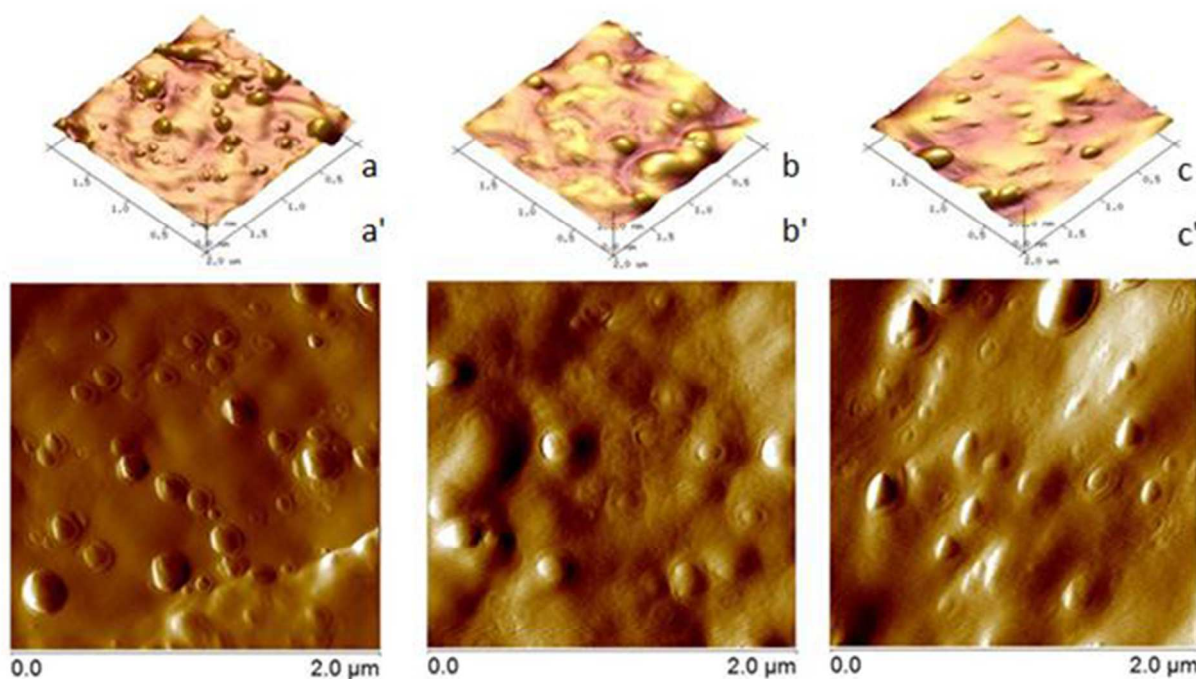
Figure 2. 3D height (up) and 2D amplitude error (down) AFM images of a, a') V-SBR-S1-35; b, b') V-SBR-S2-35; c, c') V-SBR-S5-35 nanocomposites

In the case of V-SBR-S2-35 and, mainly, V-SBR-S5-35, 3D images show less homogeneous particle dispersion (Figure 2b and 2c). Most silica particles are aggregated, showing rubber lacking zones. The aggregates are differently shaped and their image corresponds to the cross-section of the aligned anisotropic particle domains previously described by TEM, as shown in the schematic model of Figure 3.

11
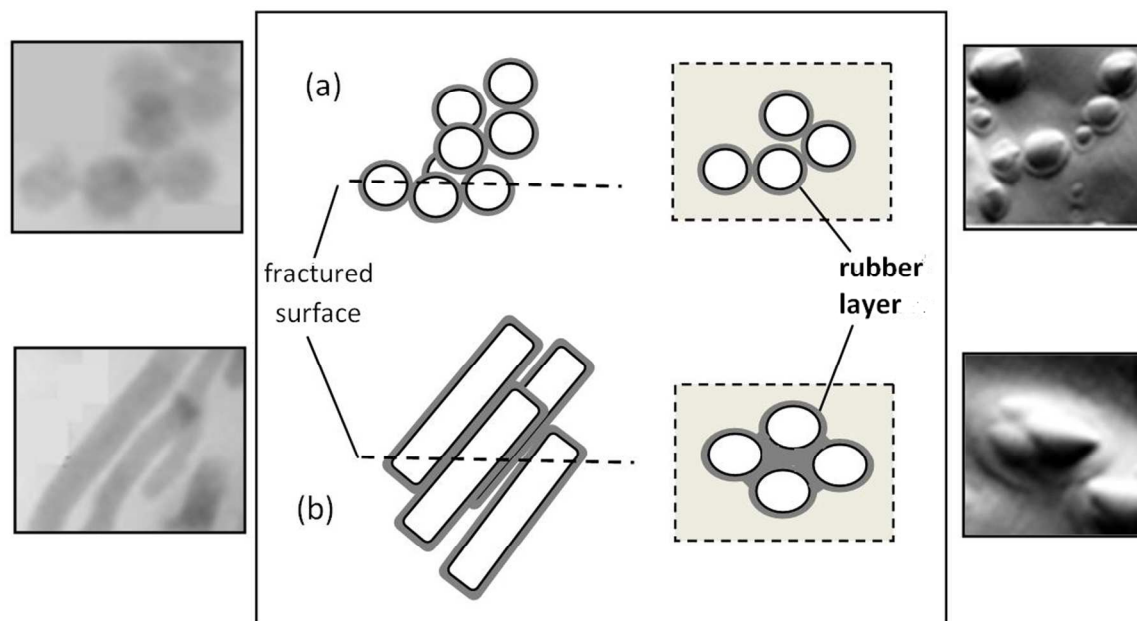
Figure 3. Model representing the aggregation of differently shaped particles and the corresponding fractured surfaces in a) V-SBR-S1-35 loaded with spherical particles and (b) V-SBR-S5-35 loaded with rod-like particles (AR=5). The models are compared with TEM (left) and 2D AFM (right) images concerning the same samples.

In fact, AFM imaging is a surface technique and the freeze-fractured specimen preparation causes the longest silica particles to be cut, lowering the probability that high AR silica particles completely lie on the fractured surface. Amplitude error images of V-SBR-S2-35 and V-SBR-S5-35 (Figure 2 b' and c') show rubber layers completely surrounding both the particle aggregates and the residual single particles in the matrix. Moreover, the aligned anisotropic particles share the rubber layers and in addition entrap a larger amount of rubber in the particle domains than the spherical ones do (Figure 3). From these observations, it seems that the particle alignment favors an enlargement of the low mobility rubber region.

In order to evaluate the thickness of the rubber layer surrounding silica particles, AFM phase images of nanocomposites were recorded. The phase signal is related to the energy dissipated by

the tapping tip while scanning the surface, and gives information at the nanometric scale about the size and the shape of local rubber heterogeneities, identifying regions with different stiffness[51-52]. According to recent studies[12,27], the thickness of the rubber layer surrounding isolated silica particles can be measured by the difference between the particle section detected in the phase images and that which is measured in the height images.

Height and phase images of V-SBR-S1-35 and V-SBR-S5-35 are reported in Figure 4 (V-SBR-S2-35 images are reported in fig. S1 of Supporting Information). For isolated nanoparticles the rubber heterogeneous layer thickness (T_r) can be calculated by the expression[12]:

$$T_r = \frac{w_{Ph} - w_{He}}{2} \qquad (1)$$

where w_{Ph} and w_{He} are the particle section widths from phase and height image, respectively, as indicated by the insets in Figure 4 (Values are reported in Table 1). In all samples the layer thickness resulted 15 ± 5 nm, irrespective of the different SX particle shapes.

The volume of heterogeneous rubber in the layers surrounding isolated silica particles can be roughly estimated by modeling the shapes of SiO_2-X as perfect spheres or cylinders having dimensions (main cross section and length) obtained by TEM and completely covered by a homogeneous rubber layer with thickness as measured by AFM . The volume was $32\pm12\%$ of the total rubber for S1, $28\pm11\%$ for S2 and $25\pm9\%$ for S5, slightly dependent on the particle shape. This confirms that the larger amount of rubber entrapped in the domains of the anisotropic silica NPs, evidenced by the AFM images (Figures 2 and 3), cannot be related to the shape of the isolated particles, but it results from the alignment of the rod-like particles. No direct indications about the different mobility of the rubber chains and, consequently, about the nature of the filler rubber interactions can be directly obtained by AFM images. They will be investigated and discussed in Time Domain NMR paragraph (3.2).

Table 1: Particles widths from height W_{He} and phase W_{Ph} images and calculated rubber layer thickness T_r.

V-SBR-S1-35			V-SBR-S2-35			V-SBR-S5-35		
w_{Ph}	w_{He}	T_r	w_{Ph}	w_{He}	T_r	w_{Ph}	w_{He}	T_r
149	180	15	63	94	15	125	157	16
143	173	15	63	99	18	134	162	14
127	155	16	64	90	13	174	215	20
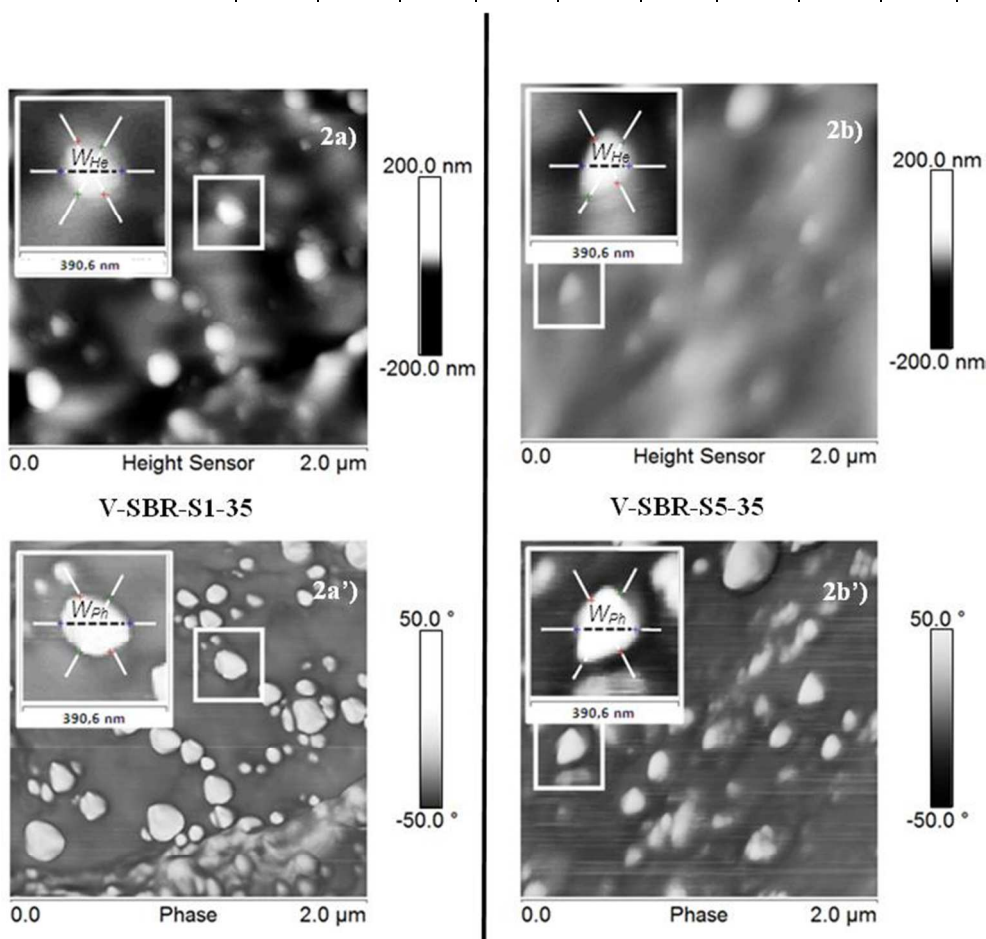
Figure 4. Height and phase images of a, a') V-SBR-S1-35 and b, b') V-SBR-S5-35 freeze-broken surfaces. The insets represent the image analysis of isolated NPs. Particle width from phase (W_{Ph}) and height (W_{He}) images are indicated.

3.2 Time domain NMR analysis

Low field TD-NMR of filled V-SBR-SX-W and of the unfilled reference V-SBR-REF-0 were used to investigate the dynamics of the polymer matrix as modified by the presence of the filler particles[53]. ^{1}H NMR MSE experiments provided information about the fractions of rubber chains having slower dynamics and they allowed correlating the dynamic behavior of the macromolecular chains with the strength of the rubber-silica interaction. The rubber was considered as composed of strongly bound chains with solid-like local mobility and of more mobile rubber phases. The estimation of the more rigid fraction was performed by quantitative detection of the signal obtained by implementing the MSE refocusing block[44,45]. Direct decomposition of the acquired FID provides the rigid fraction f_r by using the following equation[44,45]:

$$\frac{FID(t)}{FID(0)} = f_r \exp\left(-\left(\frac{t}{T_{2r}^*}\right)\right)^2 + (1 - f_r)\exp\left(-\left(\frac{t}{T_{2m}^*}\right)\right)^\nu$$

(2)

where T_{2x}^* are the apparent longitudinal relaxation times for the rigid (r) and mobile (m) phases, respectively, and ν parameterizes the deviation of the more slowly relaxing signals from purely exponential shape. Equation (2) provided very good fitting of all MSE refocused FIDs even by fixing the adjustable exponential parameter to 1, thus using a purely exponential form for the effective decay of the mobile part (See example of FID fit in Figure S2 of Supporting Information). T_{2r}^* values ranged between 22 and 30 µs at 310 K while T_{2m}^* was no less than 0.6 ms and increased with temperature (1.8 ms for V-SBR-S1-35 , 1.6 ms for V-SBR-S2-35 and V-SBR-S5-35 and 2.4 ms for the unfilled V-SBR-REF-0 at the highest temperature 393 K). The values indicate the presence of a rigid phase that could be associated either to rigid rubber or to the proton content of nanoparticles SX (*e.g.* protons of residual surface hydroxyl groups)[13]. In

15

order to isolate the fraction of rigid protons f_r^* due only to the rigid rubber in V-SBR-SX-W, the

proton content in SX $f_{r\,(SiO2)}$ was measured after removing H_2O as described in paragraph 2.4

and subtracted from the f_r values obtained by equation (2). The resulting proton content in SX

was: 1.2 % wt/wt in S1, 2.1% in S2 and 2.3% in S5 corresponding to $f_{r(SiO2)} = 0.007$, 0.014 and

0.01 in the respective V-SBR-SX-35 nanocomposites, where the total fractions of rigid protons

are $f_r = 0.072$, 0.095 and 0.098.

The amount of f_r^* of V-SBR-SX-35 as a function of temperature is shown in **Error! Reference**

source not found.5.
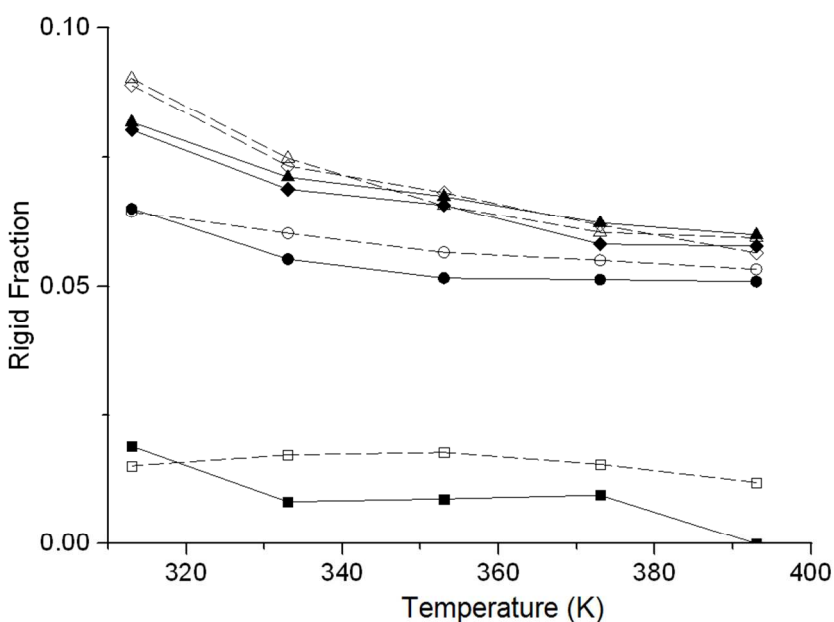
Figure 5: rigid rubber fraction f_r^* as a function of temperature of cured V-SBR-SX-35 (black

symbols) and uncured SBR-SX-35 (white symbols) nanocomposites loaded with S1 (●,○),

S2 (◆,◇) and S5 (▲, △) silica particles compared to f_r of unfilled compound V-SBR-REF-0

(■) and SBR-REF-0 (□). Lines are guides for the eye. Error bars of the rigid fraction (omitted)

are ±0.01.

The data strongly evidence that the quantity of rigid protons in the rubber surrounding silica NPs varies with the particle AR. The large amount of the rigid fraction even at $T > T_g + 100$ K, indicates a strong interaction between rubber chains and the fillers.

Considering the error ≤ 0.01 for the calculated rigid fraction[44], there is no significant difference between V-SBR-S2-35 and V-SBR-S5-35 having the highest amounts of rigid proton (respectively 8.1 % and 8.3 % of the total rubber at 313 K), while V-SBR-S1-35 loaded with spherical particles shows a lower amount of it (6.5 %). The rigid component of rubber is substantially absent in unfilled V-SBR-REF-0.

Modeling the shapes of SiO_2-X as perfect spheres or cylinders, the thickness of rigid rubber as homogeneous layer around isolated silica particles can be roughly estimated (The detailed calculation is reported in Supporting Information). It resulted 3-5.5 nm, in agreement with similar systems reported in the literature[15,54]. This thickness is associated with a primary layer of tightly bound rubber, strongly interacting with the silica particles through TESPD grafted on the silica surface[55].

The difference in the rigid fraction between spherical and rod-like particles is in principle attributable to the formation of an interparticle domain which, in the presence of anisotropic particles, immobilizes larger amounts of rubber. This result was supported by the MSE NMR experiments performed at different silica loading. In figure 6, the values of f_r^* *vs* the filler loading (expressed as volume fraction of silica in the nanocomposite) of SBR-SX-12, SBR-SX-20, SBR-SX-25 and SBR-SX-35 measured at 313 K are reported. In the composites with the lowest silica content, 12 phr, where filler particles are highly dispersed in the rubber without any alignment[34], f_r^* values are similar for both isotropic and anisotropic particles. Instead increasing

the amount of filler (20, 25 and 35 phr) the difference in f_r^* value between spherical and rod-like

shape increases.
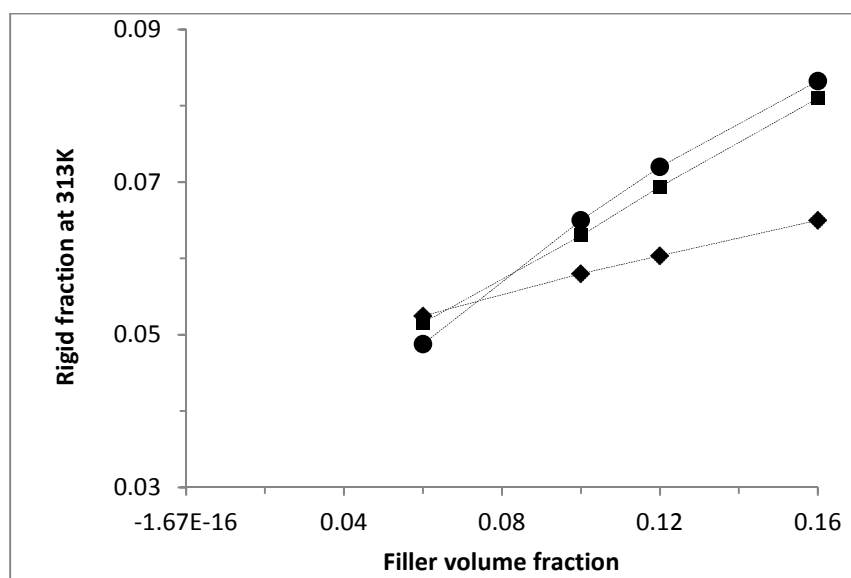
Figure 6. Rigid polymer fraction f_r^* at 313 K as a function of filler volume of V-SBR-S1-W(◆),V-SBR-S2-W (■) and V-SBR-S5-W (●) nanocomposites at different filler loading (W=12, 20, 25, 35) and of unfilled cured rubber V-SBR-REF-0 (△). Error bars of the rigid fraction (omitted) are ±0.01. Dotted lines are guides for the eye.

The non-linearity of the rigid fraction against the silica loading, may possibly be explained by

the overlap of the rubber layers of neighboring particles (both spherical and anisotropic), which

is observed also in AFM and TEM images. However, the larger amount of rigid rubber in the rod

domains compared to that in the presence of spherical particles is confirmed by the different

slopes of the f_r^* trends of V-SBR-S1-W ,V-SBR-S2-W and V-SBR-S5-W. In fact, the difference

between rod and spherical particles increases with the filler loading, in spite of the larger rubber

layer overlapping between anisotropic particles compared to spherical ones due to side

interaction (Figure 2 and 3). The difference between the fraction of the rigid rubber evaluated by

the MSE NMR, compared to that by AFM, suggests that the latter technique, which shows the size and the shape of local heterogeneous rubber zones surrounding the particles, reveals a layer constituted by both tightly rigid and more loosely interacting outermost rubber chains, cross-linked or entangled with the primary layer[17, 18].

The absence of significant difference in the rigid rubber fraction between S2 and S5 (Figure 6), indicates that the total amount of rigid rubber in the primary layers around these anisotropic fillers is about the same. Differences detected in the respective mechanical behavior (see later Paragraph 3.3) will be related to differently immobilized rubber (*e.g.* to rubber located in different particle domains).

MSE experiments were performed also on the compounds SBR-SX-35 and SBR-REF-0 before vulcanization. Interestingly, the amount of rigid rubber is very similar to that calculated for V-SBR-SX-35 (Figure 5). This confirms that the effect on the relaxation time is not due to a diffuse hardening of the rubber, but it is a local effect active even before the curing, relatable to the immobilization of the polymer chains interacting with the silica particle.

3.3 Dynamic-mechanical analysis

DMTA analyses of cured V-SBR-SX-W composites were performed in order to correlate the filler morphology to storage (G') and loss (G'') modulus and to tan δ, in the temperature range from -80 to +120 °C.
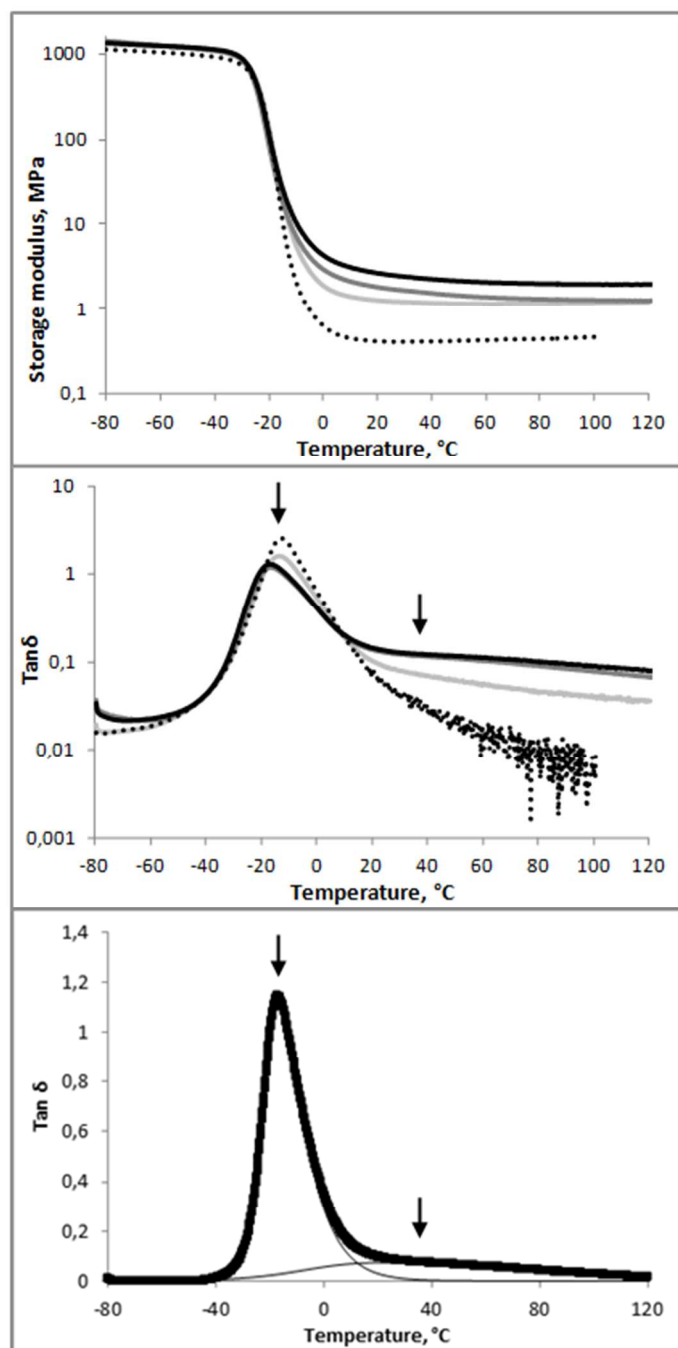
Figure 7. Plots of a) storage modulus G' and b) tan δ *vs*. temperature for V-SBR-S5-35 (full

line), V-SBR-S2-35 (—) and V-SBR-S1-35 (-) nanocomposites, and V-SBR-REF-0 (•). c)

deconvolution of tan δ *vs*.T curve of V-SBR-S5-35 sample; the two relaxation peaks (indicated

with arrows) and the sum curve (bold line) are shown.

The measurements showed the effect of rubber immobilization on the mechanical properties of the nanocomposites.

The trends of the storage modulus G' and tan δ vs temperature are plotted in Figure 7 for V-SBR-SX-35 compared with the unfilled V-SBR-REF-0. The storage modulus in the rubbery state (Figure 7 a) increases with increasing the particle AR at the same filler content in agreement with the results of a previous paper[40]. This effect was attributed to the alignment of the rod-like particles, which enhances the amount of overlapping bound rubber layers, which improve the mechanical properties[16,19]. The trend of tan δ with the temperature evidences the influence of the rubber with reduced mobility on the reinforcing effect. Plots (Figure 7 b) show a main maximum corresponding to the rubber glass transition temperature (peak 1) and a secondary relaxation peak at higher temperature (peak 2), in accordance to similar systems[35-38, 46-48]. This secondary peak is generally attributed to the rubber fraction interacting with the filler that causes a greater slowdown of polymer dynamics at the filler/rubber interface, compared to the rubber chains far from the particle interface. The stronger the interaction, the higher the peak shift. Increasing the nanoparticle AR, the intensity of the secondary relaxation peak in the region above the main glass transition increases. The trend is confirmed also for the less loaded nanocomposites V-SBR-SX-25 and V-SBR-SX-12 (plots not reported in the figure).

The values of tan δ are generally influenced by the values of the elastic modulus G'. However, as the two relaxation peaks belong to the same system, their relative area can be considered independent of G'. Therefore, even if the activation energies and the temperature dependence of the relaxation process are different, the mechanical response can be considered approximately proportional to the relative fraction of the free and reduced mobility rubber components involved in the process.

The broadening of the secondary relaxation peak is due to the distribution of the chain sequences with different mobility in the direct contact with the filler and in the outer layer. Strongly and more loosely[53] interacting fractions are evaluated altogether neglecting to consider a distribution of strength of immobilization.

Therefore, in order to estimate the amount of these rubber fractions, tan δ curves were deconvoluted into two asymmetric double sigmoid curves according to the approach of Arrighi *et al.*[56]. The amount of less mobile rubber content (R_i%) was estimated as a ratio of the area of the peak 2 with respect to the sum (peak1 + peak 2) for V-SBR-SX-W with different silica loading and different particle AR (An example of the curve deconvolution is shown in Figure 7c, while the integration results of all samples are reported in Table S2 of Supporting Information).
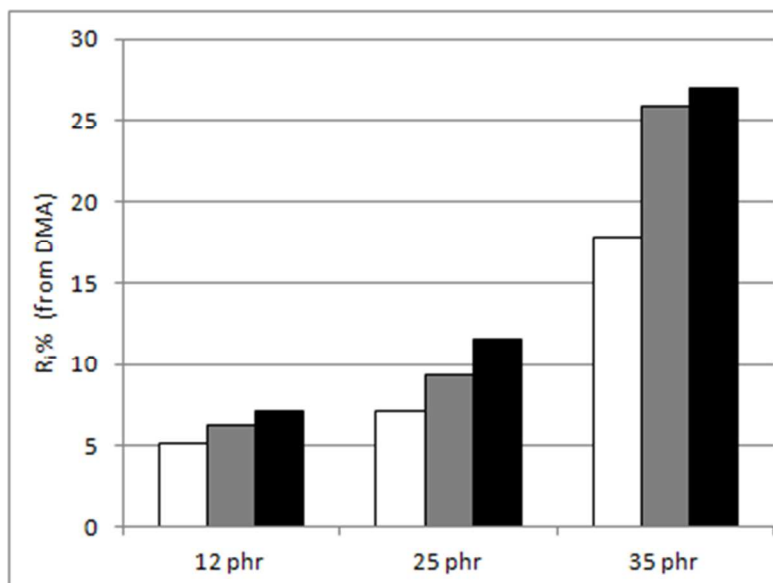
Figure 8. Percent of reduced mobility rubber (R_i%) evaluated by DMA curves integration for V-SBR-SX-W with a different silica loading and particle aspect ratio: (white) V-SBR-S1; (grey) V-SBR-S2; (black) V-SBR-S5.

The results clearly show that the total amount of rubber, tightly and loosely interacting with filler, which affect the dynamic mechanical response, increases both with the filler content and the particle AR (Figure 8), the highest values resulting for V-SBR-SX-35 in the loading range 18-27 %. It is noteworthy that in V-SBR-SX-12, where silica particles are isolated and no aggregations form, the amount of rubber with reduced mobility only slightly increases with the AR, unlike V-SBR-SX-25 and mainly V-SBR-SX-35. Even if a contribution due to a lower percolation threshold for the anisotropic particles at the highest silica loading cannot be excluded, this confirms that the self assembled long particles in the V-SBR-S2-35 and V-SBR-S5-35 composites are able to immobilize a large amount of rubber as compared to V-SBR-S1-35 containing spherical particles.
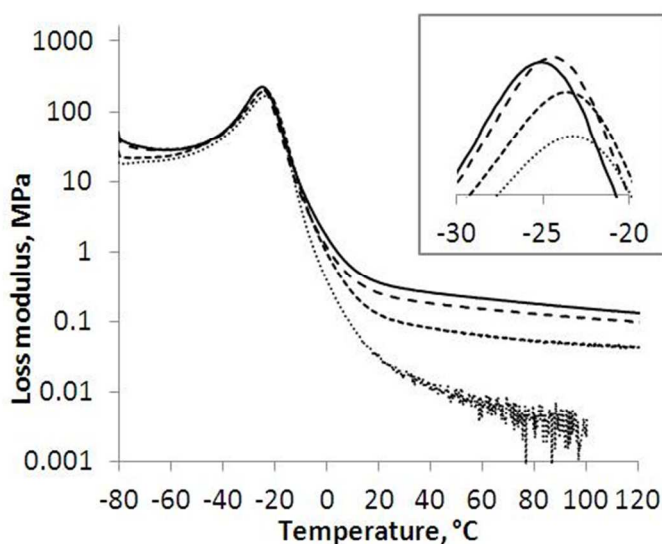
Figure 9. Plot of loss modulus against temperature for V-SBR-S5-35 (full line), V-SBR-S2-35 (—) and V-SBR-S1-35 (-) nanocomposites, and V-SBR-REF-0 (•); in the inset, a zoom on the main glass transition peak to highlight the curves maxima

The temperature dependence of the loss modulus G'' is reported in Figure 9. G'' plots allow to compare the glass transition of rubber in the composites more reliably than the tanδ plot does,

since in this case the maximum of the curve is not influenced by the value of G'. The main glass

transition gradually shifts to a lower temperature by increasing AR (inset in Figure 9). SBR- S1-

35 has a Tg = -23 °C, quite similar to that of unfilled reference V-SBR-REF-0, while V-SBR-

S2-35 and V-SBR-S5-35 have Tg of -24 and -25 °C, respectively. These results may possibly be

explained with the so called "plasticization" effect of the bulky rubber already proposed by the

literature [22,28, 57-61] to explain the different dynamics of the rubber layers remote from those close

to the constrain. According to this effect, increasing the amount of rigid rubber at the polymer

filler interface, a decrease of the packing density of the unbound bulk polymer is observed. The

increase of the free volume within the rubber matrix improves the chain freedom degree and,

consequently, reduces the glass transition temperature. In our case, the presence of an increased

fraction of low molecular weight products has been excluded in nanocomposites with high ARs

NPs. Therefore, the extent of these effects in V-SBR-S5-35 may be related due to the formation

of domains of aligned anisotropic NPs which immobilize higher rubber amount by increasing

their ARs.

3.4 Tensile tests

Tensile stress-strain tests of V-SBR-SX-35 were performed to study the material's behavior

under high deformation. Stress strain profiles and the values of elongation/stress at break are

reported in Figure 10 and Table 2.
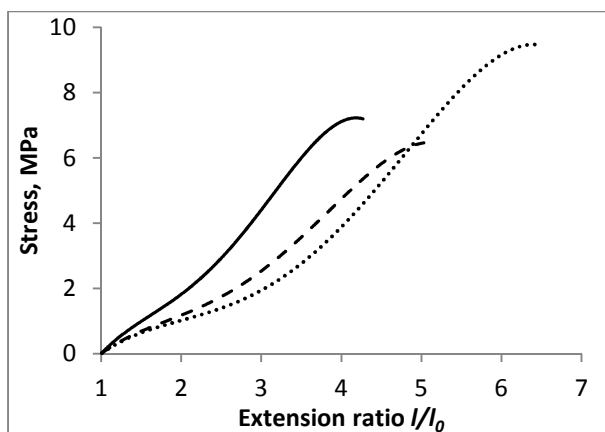
Figure 10: Tensile stress-strain profile for V-SBR-S5-35 (full line), V-SBR-S2-35 (—) and V-SBR-S1-35 (-) nanocomposites

Table 2: Stress and elongation at break from tensile stress-strain measurements for V-SBR-SX-35 nanocomposites.

	V-SBR-S1-35	V-SBR-S2-35	V-SBR-S5-35
Stress at break[MPa]	9.45	6.46	7.19
Elongation at break[%]	551	403	328

V-SBR-S5-35 showed the highest stress value for the whole strain range, confirming the higher reinforcement when increasing the particle anisotropy. On the other hand, the values of elongation at break decreased by increasing the particle AR. Therefore, in order to further investigate the tensile properties of the nanocomposites, the strain induced topological changes in the composites were studied by testing the pre-strained specimens. The so called Mullins effect describes the pre-strain induced softening. This test consists in a set of elongation-retraction cycles providing information on the changes of structure with increasing strain. The cycles of stress/strain measurements at increasing strain (from 5% to 45 %) for V-SBR-S1-35

and V-SBR-S5-35 are shown in Figure 11 a and b. The stress values of V-SBR-S5-35 samples are always higher than those of V-SBR-S1-35 at every strain value. By stepwise increasing deformation up to 25 % strain, both samples exhibit viscoelastic behavior, and the next stress-strain elongation curves (full lines in Figure 11) are superimposable with the previous ones. After the pre-strain of V-SBR-S5-35 at 30 %, the next curve shows strain softening and a lower stress value in the strain region up to 30 % due to non-Gaussian effects. This softening is the result of the filler-filler break-down and the filler-polymer contact sliding at the critical strain of 30 %. The Mullins softening is more significant in the further elongation steps at increasing strain. The area between the curves of the two subsequent elongation steps corresponds to the energy loss per volume unit at the Mullins softening. For example, V-SBR-S5-35 pre-strained at 40% results in a stress decrease ($\Delta\sigma$) with respect to the next elongation, 45%, of 40 kPa (*i.e.* 6 % of the stress value measured at the same strain, 35%) (see Fig. 11 d). This effect is much smaller in the case of V-SBR-S1-35 where the pre-strain at 40% leads to the stress softening by 15 kPa, i.e. 2.4% (see Fig. 11 c). The higher extent of strain softening in V-SBR-S5-35 implies a greater amount of reinforcing physical interactions. Moreover, both samples display a quasi-permanent deformation (tension set) 1-3 %, even after relaxation at rest, being higher in the case of V-SBR-S5-35. These results confirm that V-SBR-S5-35 filled with anisotropic particles and having a network with a higher amount of rigid rubber, presents higher stress value compared to V-SBR-S1-35. This more efficient reinforcement was proved to be brought about by stronger physical interaction broken down at the critical strain. In fact, the observed Mullins effect in the region of small strains (35-45%) is mainly a result of breaking the filler aggregates and, to a smaller extent, of an interface sliding mechanism which is dominant at higher strains[62-64].
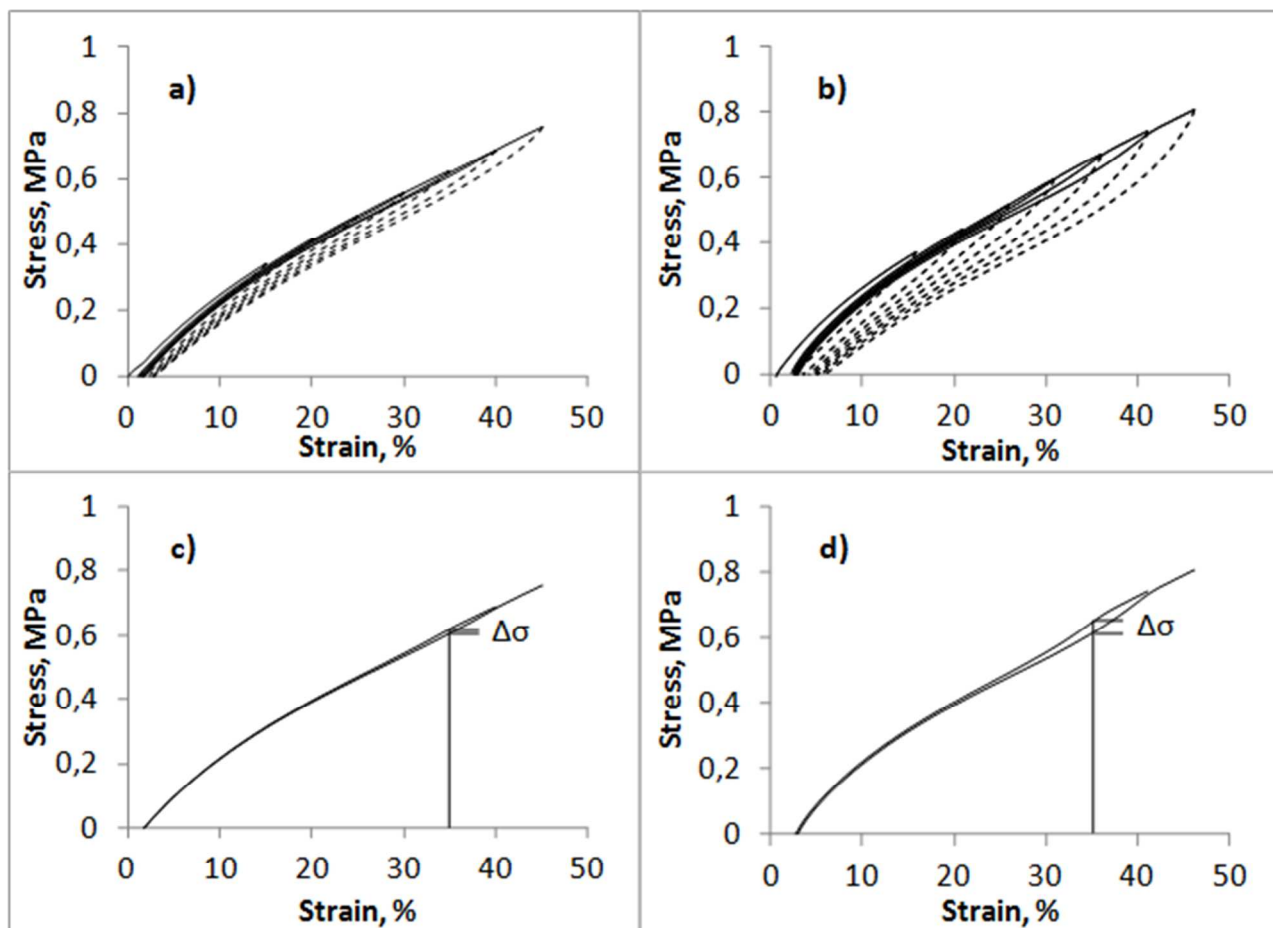
Figure 11. Loading (full line)/unloading (—) cycles for (a) V-SBR-S1-35 and (b) V-SBR-S5-35. The stress decrease ($\triangle\sigma$) measured at 35 % strain of (c) V-SBR-S1-35 and (d) V-SBR-S5-35 pre-strained at 40% and 45%.

Conclusions

Silica/SBR nanocomposites were prepared by the blending method, using shape controlled silica NPs with AR ranging from 1 to 5. These were synthesized by sol-gel route with CTAB as structure directing agent. The nanocomposites have been used as model materials to investigate the influence of the particle shape on the inorganic/organic interface and to study the effect on the dynamic-mechanical behavior of the material.

The combined use of TEM and AFM tapping mode analyses revealed that in all the V-SBR-SX-W nanocomposites, spherical and anisotropic NPs are surrounded by a layer of rubber with restricted mobility, stabilized at the particle interface. Spherical or nearly spherical particles show small contact zones sharing thin rubber layers. Rod shaped particles (AR >2) show instead oriented domains of rods preferentially aligned along the main axis, where an increase of rubber fraction trapped between the aligned particles is evident

Low field ^{1}H NMR measurements evidence that polymer chain dynamics of the rubber layers tightly bound to the silica particles are restricted by the interaction with the filler, increasing the stiffness with respect to that of polymer far from the particles. The thickness of this layer (3-5 nm) named primary one, is smaller than that detected by AFM (15±5nm), which includes also the outermost rubber chains crosslinked or entangled with the primary layer. The highest values of the rubber rigid fractions were observed in the case of anisotropic filler particles.

Dynamic-mechanical properties of V-SBR-SX-W composites show that the anisotropic rod-like particles provide stronger reinforcement of the rubber if compared with the spherical ones, increasing with the ARs. This is not related to an intrinsic property of the anisotropic particles but to the self-alignment of these particles which immobilize larger amounts of rubber in the interparticle region.

DMTA measurements evidence also that the presence of the rod-like silica domains induces a decrease of the packing density of the unbound polymer chains compared to the spherical particles, increasing the free volume in the rubber matrix and, consequently, reducing its glass transition temperature.

The strong correlation between the results of the integrated multi-technique approach allows to visualize at the nanoscale level the rubber with low mobility at the silica-rubber interface, and evidences the role of the rigid rubber on the macroscopic mechanical properties.

The study confirmed that the filler particle anisotropy is crucial to vary the amount of immobilized rubber at the filler/rubber interface and the reinforcing effect.

Acknoledgements

Electronic Supplementary Information Available

AFM roughness analysis from height images; height and phase AFM image of V-SBR-S2-35; example of curve fitting of Magic Sandwich Echo ^{1}H NMR experiment of V-SBR-SX-35; calculated integral values from simulation of tanδ *vs.* T curves of V-SBR-SX-W samples; estimation of the thickness of rigid rubber (SBR) from MSE-NMR measurements

References

(1) I. Mora-Barrantes, L. Ibarra, A. Rodrıguez, L. Gonzalez and J. L. Valentın, *J. Mater. Chem.*, 2011, **21**, 17526.

(2) *Rubber nanocomposites: preparation, properties and application*, ed. T. Sabu and S. Ranimol, Wiley-Interscience, New York, 1st edn., 2010.

(3) G. Heinrich, M. Kluppel and A.T. Vilgis, *Current Opinion Solid State Material Science,* 2002 **32**, 195–203.

(4) A.K. Bhowmick, *Current topics in elastomers research*, CRC Press–Taylor & Francis Group, Broken Sound Parkway, NW, 2008.

(5) E. Hall and J.C. Moreland, *Rubber Chem. Technol,* 2001, **74**, 525–539.

(6) D. Goritz, H. Raab, J. Frohlich and P.G. Maier, *Rubber Chem. Technol*., 1999, **72**, 929–945.

(7) J. B. Donnet, *Compos. Sci. Technol.,* 2003, **63,** 1085–1088.

(8) J. Frolich, W. Niedermeier and H.D. Luginsland, *Composite Part A Applied Science and Manufacturing,* 2005, **36**, 449–460.

(9) J. L. Leblanc *Prog. Polym. Sci.,* 2002, **27**, 627–687.

(10) R. Scotti, L. Wahba, M. Crippa, M. D'Arienzo, R. Donetti, N. Santo and F. Morazzoni, *Soft Matter,* 2012, **8,** 2131–2143.

(11) L. Wahba, M. D'Arienzo, R. Donetti, T. Hanel, R. Scotti, L. Tadiello and F. Morazzoni, *RSC Advances,* 2013, **3**, 5832.

(12) M. Qu, F. Deng, S.M. Kalkhoran, A. Gouldstone, A. Robisson and K.J. Van Vliet, *Soft Matter* 2011, **7,** 1066–1077.

(13) A. Papon, K. Saalwachter, K. Schaler, L. Guy, F. Lequeux and H. Montes *Macromolecules* 2011, **44,** 913–922.

(14) A. Kato, Y.Ikeda, R.Tsushi, R. Kokubo and N. Kojima, *Colloid Polym Sci* 2013, **291**, 2101–2110.

(15) H. Montes, T. Chaussee, A. Papon, F. Lequeux and L.Guy, *Eur. Phys. J. E,* 2010, **31,** 263–268.

(16) J. Berriot, H. Montes, F. Lequeux, D. Long and P. Sotta, *Macromolecules,* 2002, **35**, 9756–9762.

Soft Matter Accepted Manuscript

(17) S. S. Choi and E. Ko, *Polymer Testing,* 2014, **40**, 170-177.

(18) I. Pliskin and N. Tokita, *J. Appl. Polym. Sci.,* 1972, **16,** 473.

(19) L. Wahba, M. D'Arienzo, S. Dire, R. Donetti, T. Hanel, F. Morazzoni, M. Niederberger, N. Santo, L. Tadiello and R.Scotti, *Soft Matter,* 2014, **10,** 2234.

(20) A. I. Medalia, S.G. Laube, *Rubber Chemistry And Technology,* 1978, **51**, 89-109.

(21) A. I. Medalia, *Rubber Chemistry And Technology,* 1978, **51,** 437-523.

(22) R. Krishnamoorti, R. A. Vaia and E.P. Giannelis, *Chem. Mater.,* 1996, **8,** 1728-1734.

(23) Schon F., Thomann R., Gronski W., *Macromol. Symp.* **2002** 189, 105–110.

(24) Meissner B. *Rubber Chem Technol* **1995**, 68, 297-310.

(25)Braun S., Kalinowski H. O., and Berger S. *150 and more basic NMR experiments: a practical course* Wiley-VCH, 1998.

(26) Litvinov V. M. and Steeman P. A. M. *Macromolecules* **1999**, 32(25), 8476-8490.

(27) Maiti M. and Bhowmick A.K. *Polymer* **2006**, 47, 6156-6166.

(28) Schön P., Dutta S., Shirazi M., Noordermeer J., Vancso G. J. *J Mater Sci* **201**1, 46, 3507–3516.

(29) a) Pandey Y.N., Doxastakis, M, *J. Chem. Phys.* **2012,** 136, 094901 b) Pandey Y.N., Papakostantopoulos G.J., Doxastakis, M, *Macromolecules* **2013**, 46, 5097-5106.

(30) Stephanou P.S., Mavrantzas V.G., Geotgiou G.C., *Macromolecules* **2014**, 47, 4493-4513.

(31) Theodorou D.N., Vogiatzis G.G., Kritikos G. *Macromolecules* **2014**, 47, 6964-6981.

(32) Ganesan, V. and Jayaraman, *Soft Matter* **2014,** 10, 13

(33) a) Eslami H., Grmela M. and Bousmina M., *Rheol. Acta* **2009**, 48, 317-331; b) Rajabian M., Dubois C., Grmela M. *Rheol. Acta* **2005**, 44, 521-535.

Soft Matter Accepted Manuscript

(34) Robertson C. G., Lin C. J., Rackaitis M., Roland C. M., *Macromolecules* **2008**, 41, 2727-2731.

(35) Varghese S., Karger-Kocsis J., Gatos K.G., *Polymer* **2003**, 44, 3977–3983.

(36) Ramier J., Gauthier C., Chazeau L., Stelandre L., Guy L. *Journal of Polymer Science: Part B: Polymer Physics* **2007**, 45, 286–298.

(37) Bindu P., Thomas S. *J. Phys. Chem. B* **2013**, 117, 12632−12648.

(38) Fragiadakis D., Bokobza L., Pissis P., *Polymer* **2011**, 52, 3175-3182.

(39) Gao et al. Phys. Chem. Chem. Phys., 16, 21372 (2014)

(40) Scotti R., Conzatti L., D'Arienzo M., Di Credico B., Giannini L., Hanel T., Stagnaro P., Susanna A., Tadiello L., Morazzoni F., *Polymer* **2014**, 55, 1497-1506.

(41) Tsagaropoulos G., Eisenberg A., *Macromolecules* **1994**, 28, 6067-6077.

(42) Tsagaropoulos G., Eisenberg A, *Macromolecules* **1996**, 28, 396-398.

(43) Du X., He J. *Dalton Trans.* **2010**, 39, 9063-9072.

(44) Maus A., Hertlein C., Saalwächter K. *Macromolecular Chemistry and Physics* **2006**, 207, 1150-1158.

(45) Mauri M., Thomann Y., Schneider H., Saalwächter K. *Solid State Nuclear Magnetic Resonance* **2008**, 34, 125-141.

(46) Mauri M, Mauri L, Causin V, Simonutti R., *Analytical Methods* **2011,** 3, 1802-9

(47) Diani J., Fayolle B., Gilormini P., *European Polymer Journal* **2009**, 601-612.

(48) Schmoller K. M., Bausch A. R., *Nature Materials* **2013**, 278-281.

(49) Hu X., Littrel K., Jia S., Pickles D.G., Risen Jr W.M., *Journal of Non-Crystalline Solids* **2001**, 184-190.

(50) Brewer A. K., Striegel A. M. *Analytical chemistry* **2011**, 83, 3068–3075.

Soft Matter Accepted Manuscript

(51) Di Nardo N. J., *Nanoscale Characterization of Surfaces and Interfaces*, VCH, 1994.

(52) Špírková M., Pavličević J., Strachota A., Poreba R., Bera O., Kaprálková L., Baldrian J., Šlouf M., Lazić N., Budinski-Simendić J., *European Polymer Journal* **2011**, 47, 959-972.

(53) Papon A., Saalwachter K., Schaler K., Guy L., Lequeux F., Montes H. *Macromolecules* **2011**, 44(4), 913-922.

(54) Mujtaba A., Keller M., Ilisch S., Radusch H. J., Beiner M., Thurn-Albrecht T., Saalwachter K., *ACS Macro Lett*. **2014**, 3, 481.

(55) Valentín J. L*.,* Mora-Barrantes I., Carretero-González J., López-Manchado M. A., Sotta P., Long D. R., Saalwächter K., *Macromolecules* **2010**, 43, 334.

(56) Arrighi V., McEwen I.J., Qian H., Serrano Prieto M.B., *Polymer* **2003**, 44, 6259–6266.

(57) Barut G., Pissis P., Pelster R., Nimtz G., *Phys Rev Lett* **1998**, 80, 3543.

(58) Daoukaki D., Barut G., Pelster R., Nimtz G., Kyritsis A., Pissis P., *Physical Review B* **1998**, 58,5336.

(59) Gorbatschov W., Arndt A., Stannarus R., Kremer F., *Europhys Lett* **1996**, 35, 719.

(60) DeMaggio G. B., Frieze W. E., Gidley D., Minz Z., Hristov H. A., Yee A. F., *Phys Rev Lett* **1997**, 78, 1524.

(61) Bershtein V.A., Egorova L.M., Yakushev P.N., Pissis P., Sysel P., Brozova L., *J. Polym.Sci. : Part B: Polym. Phys.* **2002**, 40,1056–1069.

(62) Bokobza L. *Rubber Chemistry And Technology* **2013**, 86, 423–448.

(63) Meissner B., Matejka L., *Polymer* **2006**, 47, 7997-8012.

(64) Fukahori Y., *J. Appl. Polym. Sci.* **2005**, 95, 60–67.

Filler-Rubber Interface in Styrene Butadiene Nanocomposites with Anisotropic Silica Particles. Morphology and Dynamic Properties.

L. Tadiello[a], M.D'Arienzo[a], B.Di Credico[a], T. Hanel[b], L. Matejka[c], M. Mauri[a], F.Morazzoni[a],

R.Simonutti[a], M. Spirkova,[c] R. Scotti[a] *

For Table of Contents use only
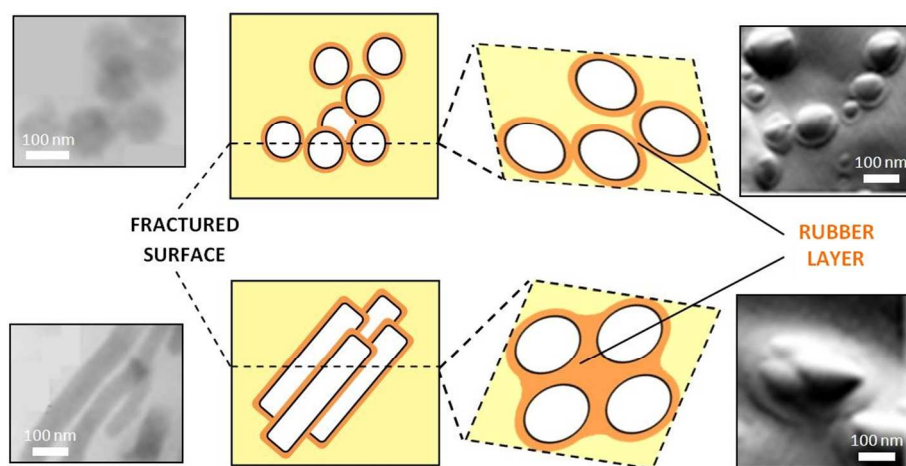
In SBR/silica nanocomposites the amount of immobilized rubber is higher with rod-like filler particles which self-align compared to spherical ones, improving the rubber reinforcing.

34